

# Four-wave mixing model solutions for polarization control of terahertz pulse generated by a two-color laser field in air

Zheng Chu (褚政)<sup>1</sup>, Jinsong Liu (刘劲松)<sup>1\*</sup>, Kejia Wang (王可嘉)<sup>1</sup>, and Jianquan Yao (姚建铨)<sup>1,2</sup>

<sup>1</sup>Wuhan National Laboratory for Optoelectronics, School of Optoelectronic Science and Engineering, Huazhong University of Science and Technology, Wuhan 430074, China

<sup>2</sup>College of Precision Instrument and Opto-Electronics Engineering, Tianjin University, Tianjin 300072, China

\*E-mail: jslu4508@vip.sina.com

Received February 10, 2010

A four-wave mixing (FWM) model is used to analyze the polarization control of terahertz (THz) pulse generated by a two-color laser field in air. The analytic formula for the THz intensity varying with the THz polarizer angle, and the relative phase between the two pulses, are obtained. The corresponding numerical results agree well with both numerical result obtained from a quantum model and measured data reported. Moreover, possible phenomena are predicted for variables not found in other experiments. Compared with the quantum model, the FWM model gives analytic formulas and clear physical pictures, and has the advantage of efficient computing time.

OCIS codes: 190.7110, 300.6495, 190.4380.

doi: 10.3788/COL20100807.0697.

Terahertz (THz) waves can be efficiently produced by femtosecond (fs) laser filament. They have many applications, such as remote-sensing, chemical spectroscopy, biomedical diagnostics, threat detection, and imaging<sup>[1–5]</sup>. Four-wave mixing (FWM) models have been offered to account for THz generation by mixing an optical fundamental wave ( $\omega$ ) with its second-harmonic wave ( $2\omega$ )<sup>[6]</sup>. Thus, investigations describing the polarization and intensity of THz waves have been conducted<sup>[7–9]</sup>. Recently, a quantum model has been applied to describe THz generation in two-color laser field<sup>[10]</sup>. Lately, two groups of researchers have independently conducted experiments to reveal the polarization characteristics of THz waves generated from gas plasma excited by dual-color optical pulses<sup>[11,12]</sup>. It was found that the polarization of THz waves could be controlled by changing the phase between  $\omega$  and  $2\omega$  pulses when at least one of the optical pulses was elliptically polarized. In particular, when both beams were circularly polarized, the THz polarization angle could be rotated arbitrarily by simply changing the phase between the two optical pulses while keeping the THz amplitude constant. These experimental findings can be completely reproduced by numerical simulation based on the quantum model<sup>[10]</sup>. A natural question, however, concerns whether these findings can be explained based on the FWM model. As presented in this letter, we develop the standard FWM model to describe the above-mentioned experimental findings. Numerical simulation results show the capability to completely reproduce the experimental findings and predict possible phenomena that have not been found in any other experiments. Compared with the quantum model, the FWM model can derive analytic formulas and has the advantage of efficient computing time.

The present theoretical work employs experimental conditions according to Ref. [11]. Figure 1 shows the diagrammatic sketch of coordinates. Pulses propagate along the  $z$ -axis. The  $x$ - and  $y$ -axis are parallel to  $e$ - and  $o$ -axis of the BBO crystal, respectively. The  $\omega$  and  $2\omega$

pulses can be written as

$$\mathbf{E}_\omega = \mathbf{E}_\omega^x \mathbf{e}_x + \mathbf{E}_\omega^y \mathbf{e}_y = A_\omega^x(t, \tau_1) e^{-i[\omega_1(t-\tau_1)-k_1z]} \mathbf{e}_x + A_\omega^y(t, \tau_1) e^{-i[\omega_1(t-\tau_1)-k_1z \pm \frac{\pi}{2}]} \mathbf{e}_y + c.c., \quad (1a)$$

$$\mathbf{E}_{2\omega} = \mathbf{E}_{2\omega}^x \mathbf{e}_x + \mathbf{E}_{2\omega}^y \mathbf{e}_y = A_{2\omega}^x(t, \tau_2) e^{-i[\omega_2(t-\tau_2)-k_2z]} \mathbf{e}_x + A_{2\omega}^y(t, \tau_2) e^{-i[\omega_2(t-\tau_2)-k_2z \pm \frac{\pi}{2}]} \mathbf{e}_y + c.c., \quad (1b)$$

where  $\tau_1$  and  $\tau_2$  are the time delays of  $\omega$  and  $2\omega$  pulses when they pass through quartz wedges; phase  $\pm \frac{\pi}{2}$  in the exponential term indicates the rotation direction of  $\omega$  and  $2\omega$  pulses, which takes a positive or negative value depending on the direction of the pulses (i.e., right- or left-hand circularly polarized); and  $A^x$  and  $A^y$  denote the amplitudes of the optical fields in the  $x$  and  $y$  directions, respectively. The relative time delay between the two pulses can be written as  $\Delta\tau = \tau_1 - \tau_2$ .

By assuming that the envelope of the  $\omega$  pulse amplitude obeys a Gaussian distribution, and by denoting  $t = 0$  as the moment when the peak of the pulse arrives to the detector, we can obtain  $A_\omega(t) = A_\omega e^{-\frac{1}{2}(\frac{t}{\tau})^2}$ , where  $\tau$  is pulse duration and is taken as 25 fs. Since the  $2\omega$  pulse is generated by second-harmonic generation in the BBO crystal<sup>[8]</sup>, thus  $A_{2\omega}(t) \propto A_\omega^2(t)$  such that

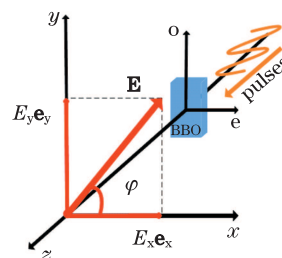


Fig. 1. Diagrammatic sketch of coordinates. Pulses propagate along the  $z$ -axis. The  $x$ - and  $y$ -axis are parallel to the  $e$ - and  $o$ -axis of the BBO crystal, respectively. Any optical field  $\mathbf{E}$  can be divided into  $E_x \mathbf{e}_x$  and  $E_y \mathbf{e}_y$ , where  $\mathbf{e}_x$  and  $\mathbf{e}_y$  are the unit length vectors of the  $x$ - and  $y$ -axis, respectively.

$A_{2\omega}(t) = A_{2\omega}e^{-\left(\frac{t}{\tau}\right)^2}$ . When delays are considered, we can obtain  $A_{\omega}(t, \tau_1) = A_{\omega}e^{-\frac{1}{2}\left(\frac{t-\tau_1}{\tau}\right)^2}$  and  $A_{2\omega}(t, \tau_2) = A_{2\omega}e^{-\left(\frac{t-\tau_2}{\tau}\right)^2}$ . By assuming that the THz pulse can be detected at  $t = \tau_1$ , the envelope of the product of the filed amplitudes can then be given by

$$A_{\omega}^2(t, \tau_1)A_{2\omega}(t, \tau_2)|_{t=\tau_1} = A_{\omega}^2A_{2\omega}e^{-\left(\frac{\phi}{2\omega\tau}\right)^2}, \quad (2)$$

where  $\phi = 2\omega_1\tau_1 - \omega_2\tau_2 \approx 2\omega\Delta\tau$  is the relative phase between  $\omega$  and  $2\omega$  pulses, and  $\Delta\tau$  is caused by dispersion in both optical devices and air<sup>[11]</sup>.

If we let  $E_{\text{THz}}$  denote the field amplitude of THz beam, the FWM model will derive  $E_{\text{THz}}^i \propto \sum_{jkl} \chi_{ij}^{lk} (E_{2\omega}^j)^* E_{\omega}^k E_{\omega}^l$  ( $i, j, k, l = x, y$ ), where  $\chi_{ijkl}$  is the

$$\begin{aligned} \mathbf{E}_{\text{THz}} \propto & (\chi_{xxxx}A_{\omega}^xA_{\omega}^xA_{2\omega}^x + \chi_{xyxy}A_{\omega}^yA_{\omega}^xA_{2\omega}^y)e^{-\left(\frac{\phi}{2\omega\tau}\right)^2} \cos(\phi_0 + \phi)\mathbf{e}_x \\ & + (\chi_{yyyy}A_{\omega}^yA_{\omega}^yA_{2\omega}^y + \chi_{yxxy}A_{\omega}^xA_{\omega}^yA_{2\omega}^x)e^{-\left(\frac{\phi}{2\omega\tau}\right)^2} \sin(\phi_0 + \phi)\mathbf{e}_y, \end{aligned} \quad (3)$$

where  $\phi_0 = \omega_{\text{THz}}t - k_{\text{THz}}z$ ,  $\omega_{\text{THz}} = 2\omega_1 - \omega_2$  is the angular frequency of the THz pulse, and  $k_{\text{THz}} = 2k_1 - k_2$ . It should be noted that  $\phi_0$  is taken as a constant in the said calculation. The relationship in the third order susceptibility tensors is  $\chi_{xxxx} = \chi_{yyyy}$  and  $\chi_{xyxy} = \chi_{yxxy}$ <sup>[13]</sup>.

When a broadband THz polarizer is used to analyze the polarization of the emitted THz waves, the output THz waves are

$$\begin{aligned} \mathbf{E}_{\text{out}} = \mathbf{E}_{\text{THz}} \cdot \mathbf{e}_p \propto & e^{-\left(\frac{\phi}{2\omega\tau}\right)^2} (\chi_{xxxx}A_{\omega}^xA_{\omega}^xA_{2\omega}^x + \chi_{xyxy}A_{\omega}^yA_{\omega}^xA_{2\omega}^y)e^{-\left(\frac{\phi}{2\omega\tau}\right)^2} \cos(\phi_0 + \phi) \cos\theta \mathbf{e}_x \\ & + (\chi_{yyyy}A_{\omega}^yA_{\omega}^yA_{2\omega}^y + \chi_{yxxy}A_{\omega}^xA_{\omega}^yA_{2\omega}^x)e^{-\left(\frac{\phi}{2\omega\tau}\right)^2} \sin(\phi_0 + \phi) \sin\theta \mathbf{e}_y, \end{aligned} \quad (4)$$

where  $\mathbf{e}_p$  is the unit vector representing the polarization direction of the THz polarizer, and  $\theta$  is the angle between  $\mathbf{e}_p$  and  $\mathbf{e}_x$ . Thus, the THz intensity that can be detected is

$$\begin{aligned} I_{\text{out}} \propto & |e^{-\left(\frac{\phi}{2\omega\tau}\right)^2} [(\chi_{xxxx}A_{\omega}^xA_{\omega}^xA_{2\omega}^x + \chi_{xyxy}A_{\omega}^yA_{\omega}^xA_{2\omega}^y)e^{-\left(\frac{\phi}{2\omega\tau}\right)^2} \cos(\phi_0 + \phi) \cos\theta \\ & \mp (\chi_{yyyy}A_{\omega}^yA_{\omega}^yA_{2\omega}^y + \chi_{yxxy}A_{\omega}^xA_{\omega}^yA_{2\omega}^x)e^{-\left(\frac{\phi}{2\omega\tau}\right)^2} \sin(\phi_0 + \phi) \sin\theta]|^2. \end{aligned} \quad (5)$$

When  $\omega$  and  $2\omega$  pulses are set for parallel and linear polarizations,  $A_{\omega}^y$  and  $A_{2\omega}^y$  can be set to zero. Expression (5) becomes

$$I_{\text{out}} \propto |e^{-\left(\frac{\phi}{2\omega\tau}\right)^2} \chi_{xxxx}A_{\omega}^xA_{\omega}^xA_{2\omega}^x \cos(\phi_0 \pm \phi) \cos\theta|^2. \quad (6)$$

Figure 2(a) shows the curves of  $I_{\text{out}}$  versus both  $\theta$  and  $\phi$ , which agree well with both numerical results obtained from the quantum model and the measured results. These are shown in Ref. [11].

When both  $\omega$  and  $2\omega$  beams are right-hand circularly polarized,  $A_{\omega}^x = A_{\omega}^y = A_{\omega}$ ,  $A_{2\omega}^x = A_{2\omega}^y = A_{2\omega}$ , and  $\chi_{xxxx} + \chi_{xyxy} = \chi_{yyyy} + \chi_{yxxy} = \chi$  are obtained. In this case, the expression of  $I_{\text{out}}$  is

$$I_{\text{out}} \propto |e^{-\left(\frac{\phi}{2\omega\tau}\right)^2} \chi A_{\omega}^2 A_{2\omega}|^2 \cos^2(\phi_0 + \phi - \theta). \quad (7)$$

The numerical results for  $I_{\text{out}}$ , which change with both  $\theta$  and  $\phi$ , are shown in Fig. 3(a). These also agree well with both the numerical results obtained from the quantum model as well as the measured results in Ref. [11]. The polarization of the emitted THz beam rotates while the intensity or the electric field of the THz wave is kept unchanged. This phenomenon can be explained by the analytical formula of Eq. (7). It should be noted that the THz intensity is in proportion with  $\cos^2(\phi_0 + \phi - \theta)$ , thus the output intensity does not change as the difference between  $\phi$  and  $\theta$  is a constant, particularly when  $\phi$

third order nonlinear susceptibility tensor of air. In the expression in Refs. [7,11], the subscript  $i$  corresponds to the THz wave, subscript  $j$  corresponds to the  $2\omega$  pulse, and the subscripts  $k$  and  $l$  correspond to the  $\omega$  pulse. The case of  $\omega$  and  $2\omega$  pulses perpendicularly and linearly polarized shall be discussed in later segments of this letter. First, we consider cases wherein the  $\omega$  and  $2\omega$  pulses are circularly or elliptically polarized, or parallel linearly polarized. For these cases, although many terms for  $\chi_{ijkl}$  are available, the four terms of  $\chi_{xxxx}$ ,  $\chi_{yyyy}$ ,  $\chi_{xyxy}$ , and  $\chi_{yxxy}$  are commonly used compared with other terms ( $\chi_{xxyy}$ ,  $\chi_{yyxx}$ ,  $\chi_{xyxx}$ ,  $\chi_{yxyy}$ ,  $\chi_{xyyy}$ , and  $\chi_{yxxx}$ )<sup>[7,8,13]</sup>. We only consider the contribution from the four terms. Thus, the vectorial THz field is expressed as

is not large enough in relation to  $e^{-\left(\frac{\phi}{2\omega\tau}\right)^2} \approx 1$ . The FWM model shows an obvious advantage over the quantum model, which can be obtained from the analytical formula for the output THz intensity. When  $\omega$  pulse is circularly polarized and  $2\omega$  pulse is left- or right-hand elliptically polarized,  $A_{\omega}^x = A_{\omega}^y = A_{\omega}$  and  $A_{2\omega}^x = \sqrt{11}A_{2\omega}^y = A_{2\omega}$  are set with ellipticity of about 1/11 in terms of optical intensity<sup>[11]</sup>. Similarly, we use  $\chi_{xxxx} = \chi_{yyyy} = 0.4\chi_{xyxy} = 0.4\chi_{yxxy}$ <sup>[8]</sup>. In this case, the expression of  $I_{\text{out}}$  is

$$\begin{aligned} I_{\text{out}} \propto & |e^{-\left(\frac{\phi}{2\omega\tau}\right)^2} A_{\omega}A_{\omega}A_{2\omega} [ \left( \chi_{xxxx} + \frac{1}{2}\chi_{xyxy} \right) \\ & \cdot \cos(\phi_0 + \phi) \cos\theta - \left( \frac{1}{2}\chi_{yyyy} + \chi_{yxxy} \right) \\ & \cdot \sin(\phi_0 + \phi) \sin\theta ]|^2 \end{aligned} \quad (8a)$$

if the  $2\omega$  pulse is left-handed, and

$$\begin{aligned} I_{\text{out}} \propto & |e^{-\left(\frac{\phi}{2\omega\tau}\right)^2} A_{\omega}A_{\omega}A_{2\omega} [ \left( \chi_{xxxx} + \frac{1}{\sqrt{11}}\chi_{xyxy} \right) \\ & \cdot \cos(\phi_0 + \phi) \cos\theta + \left( \frac{1}{\sqrt{11}}\chi_{yyyy} + \chi_{yxxy} \right) \\ & \cdot \sin(\phi_0 + \phi) \sin\theta ]|^2 \end{aligned} \quad (8b)$$

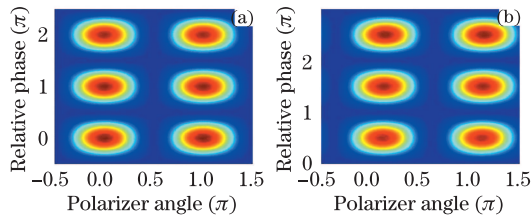


Fig. 2. THz intensity versus THz polarizer angle  $\theta$  and relative phase  $\phi$  between  $\omega$  and  $2\omega$  pulses with (a) parallel and (b) perpendicular linear polarization.

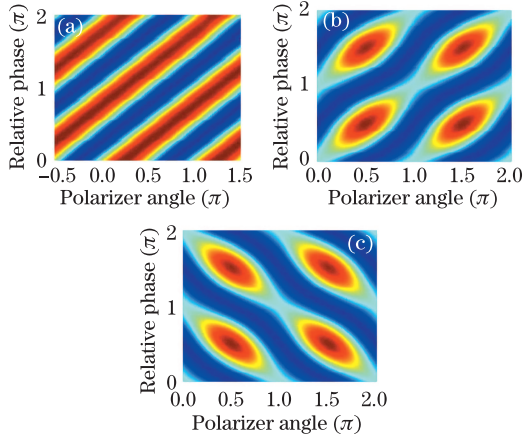


Fig. 3. THz intensity versus the THz polarizer angle  $\theta$  and relative phase  $\phi$ . (a) Both  $\omega$  and  $2\omega$  pulses are right-hand circularly polarized. The  $\omega$  pulse is circularly polarized, and the  $2\omega$  pulse is (b) right-hand and (c) left-hand elliptically polarized.

if the  $2\omega$  pulse is right-handed. Figures 3(b) and (c) show the simulation results when the  $\omega$  pulse is left- or right-hand circularly polarized and the  $2\omega$  pulse is elliptically polarized. The findings agree with numerical results obtained from the quantum model, as well as with measured results as shown in Ref. [11].

As mentioned earlier, we now discuss the case where  $\omega$  and  $2\omega$  pulses are perpendicular and linearly polarized. The case is different under these conditions. The cross terms of  $\chi_{ijkl}$  are first considered. By letting  $A_\omega^y = A_{2\omega}^y = 0$ , only the two terms of  $\chi_{xyxx}$  and  $\chi_{yyxx}$  are considered. In Fig. 3 of Ref. [7], the trace of  $\chi_{yyxx}$  is obviously asymmetrical with respect to  $\Delta\tau = 0$  ( $x$ -axis). Based on this experimental observation, we assume that there will be a delay time  $\tau_0$  for the term  $\chi_{yyxx}$  compared with the item on  $\chi_{xyxx}$  for the relation of  $\chi_{ijkl}$  varying with  $\Delta\tau$ . As a result, the output THz intensity is written as

$$I_{\text{out}} \propto |e^{-2(\frac{\phi}{2\omega\tau})^2} \chi_{xyxx} A_\omega^x A_\omega^x A_{2\omega}^y \sin(\phi_0 + \phi) \cos \theta + e^{-2(\frac{\phi - 2\omega\tau_0}{2\omega\tau})^2} \chi_{yyxx} A_\omega^x A_\omega^x A_{2\omega}^y \sin(\phi_0 + \phi) \sin \theta|^2, \quad (9)$$

where  $\tau_0$  is the trace delay in the  $yyxx$  polarization mode as compared with the  $xyxx$  polarization mode<sup>[7]</sup>. The  $yyxx$  or  $xyyy$  mode is different from the other modes. In these two modes, THz is perpendicular to all  $\omega$  pulses but parallel to  $2\omega$  pulse. The  $2\omega$  pulse can affect THz generation more directly than the  $\omega$  pulse for the parallel relationship. If there is a delay ( $\tau_0 > 0$ ), the  $\omega$  pulse leads to  $2\omega$  pulse; then, the  $\omega$  pulse ionizes the air and loses part of its energy, unlike for  $2\omega$  pulse which does

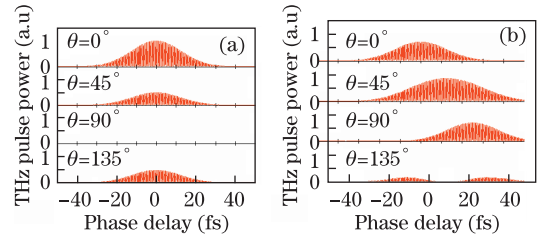


Fig. 4. THz intensity versus the relative phase between  $\omega$  and  $2\omega$  pulses with (a) parallel and (b) perpendicular linear polarization.

not lose any. Since THz pulse is sensitive to  $2\omega$  pulse, the peak of THz generation is at  $t = \tau_0$ . The half-width at half-maximum (HWHM) of  $\tau$  is about 25 fs (defined by Fig. 2 in Ref. [7]), which allows for  $\tau_0 \approx 25$  fs. It is then assumed that  $\chi_{xyxx} \approx \chi_{yyxx}$ <sup>[7]</sup>. Another relationship  $\chi_{xyxx} \approx 2\chi_{yyxx}$  may have been presented<sup>[13]</sup>. It is not necessary to identify which among these is more accurate; ultimately, the following variation tendency is not affected.

The numerical results are shown in Fig. 2(b). Figures 2(a) and (b) seem similar at a glance. A closer analysis will reveal a difference in the forms of THz intensity varying with  $\phi$ . This difference is created by the second term in Eq. (9), which originates from the delay of  $\chi_{yyxx}$ . Figure 4 shows the curves of the THz intensity varying with  $\phi$  at different values of the polarizer angle. When  $\theta = 0^\circ$ , the curves have the same form as the parallel and perpendicular linear polarization. When  $\theta = 45^\circ$ , a delay for the perpendicular case is produced although the curves have the same forms. When  $\theta = 90^\circ$ , output power for the parallel case is absent while a large delay for the perpendicular case is produced. When  $\theta = 135^\circ$ , the curve for the perpendicular case is a double hill structure, which is different from that of the parallel case. These elaborate descriptions for the perpendicular case have not been confirmed experimentally, hence necessitating a corresponding experiment.

In conclusion, this letter presents a theoretical investigation on the polarization characteristics of the THz waves generated from the gas plasma excited by dual-color optical pulses in an FWM model. Based on this, we have derived a simple analytic formula for the THz intensity that varies with the THz polarizer angle and the relative phase between the two pulses. Numerical results from the FWM model agree well with both the numerical results obtained from the quantum model, as well as the measured results. Moreover, some new phenomena have been proposed, which need to be further validated by suitable experiments.

This work was supported by the National Natural Science Foundation of China (No. 10974063), the Research Foundation of Wuhan National Laboratory (No. P080008), and the National “973” Program of China (No. 2007CB310403).

## References

1. Q. Wu and X.-C. Zhang, Appl. Phys. Lett. **67**, 3523 (1995).
2. J. H. Booske, Physics of Plasmas **15**, 055502 (2008).
3. P. H. Siegel, IEEE Trans. Microw. Theor. Tech. **50**, 910 (2002).

4. Y. Zhang, Y. Chen, C. Marceau, W. Liu, Z. D. Sun, S. Xu, F. Théberge, M. Châteauneuf, J. Dubois, and S. L. Chin, *Opt. Express* **16**, 15483 (2008).
5. Y. He, Y. Jiang, Y. Zhang, and G. Fan, *Chin. Opt. Lett.* **8**, 162 (2010).
6. D. J. Cook and R. M. Hochstrasser, *Opt. Lett.* **25**, 1210 (2000).
7. X. Xie, J. Dai, and X.-C. Zhang, *Phys. Rev. Lett.* **96**, 075005 (2006).
8. Y. Zhang, Y. Chen, S. Xu, H. Lian, M. Wang, W. Liu, S. L. Chin, and G. Mu, *Opt. Lett.* **34**, 2841 (2009).
9. N. Amer, W. C. Hurlbut, B. J. Norton, L. Yun-Shik, and T. B. Norris, *Appl. Phys. Lett.* **87**, 221111 (2005).
10. N. Karpowicz and X.-C. Zhang, *Phys. Rev. Lett.* **102**, 093001 (2009).
11. J. Dai, N. Karpowicz, and X.-C. Zhang, *Phys. Rev. Lett.* **103**, 023001 (2009).
12. H. Wen and A. M. Lindenberg, *Phys. Rev. Lett.* **103**, 023902 (2009).
13. A. Houard, Y. Liu, B. Prade, and A. Mysyrowicz, *Opt. Lett.* **33**, 1195 (2008).